



# CHORUS

This is the accepted manuscript made available via CHORUS. The article has been published as:

## Evolution of electronic correlations across the rutile, perovskite, and Ruddelsden-Popper iridates with octahedral connectivity

Jason K. Kawasaki, Masaki Uchida, Hanjong Paik, Darrell G. Schlom, and Kyle M. Shen

Phys. Rev. B **94**, 121104 — Published 6 September 2016

DOI: [10.1103/PhysRevB.94.121104](https://doi.org/10.1103/PhysRevB.94.121104)

# Evolution of electronic correlations across the rutile, perovskite, and Ruddlesden-Popper iridates with octahedral connectivity

Jason K. Kawasaki,<sup>1,2,3</sup> Masaki Uchida,<sup>4</sup> Hanjong Paik,<sup>2</sup> Darrell G. Schlom,<sup>2,3</sup> and Kyle M. Shen<sup>1,3,\*</sup>

<sup>1</sup>Laboratory for Atomic and Solid State Physics, Cornell University, Ithaca NY 14853

<sup>2</sup>Department of Materials Science and Engineering, Cornell University, Ithaca NY 14853

<sup>3</sup>Kavli Institute at Cornell for Nanoscale Science, Cornell University, Ithaca NY 14853<sup>†</sup>

<sup>4</sup>Department of Applied Physics, University of Tokyo, Tokyo Japan

(Dated: August 16, 2016)

The confluence of electron correlations and spin-orbit interactions is critical to realizing novel quantum phases in  $5d$  transition metal oxides. Here, we investigate how the strength of the effective electron correlations evolve across a series of  $d^5$  iridates comprised of  $\text{IrO}_6$  octahedra, ranging from the layered correlated insulator  $\text{Sr}_2\text{IrO}_4$ , to the three dimensional perovskite semimetal  $\text{SrIrO}_3$ , to metallic rutile  $\text{IrO}_2$  in which the octahedra are arranged in a mixed edge and corner sharing network. Through a combination of reactive oxide molecular-beam epitaxy, *in situ* angle-resolved photoemission spectroscopy, core level photoemission, and density functional theory, we show how the effective electron correlations weaken as a function of increasing connectivity of the  $\text{IrO}_6$  network and  $p-d$  hybridization. Our results demonstrate how structure and connectivity can be used to control the strength of correlations in the iridates.

Electron-electron correlations play an essential role in renormalizing the ground state of many transition metal oxides. While this renormalization was once thought to be weak in the late transition metals due to the extended spatial extent of  $5d$  orbitals, it is now well appreciated that spin-orbit coupling can enhance the effects of correlations, particularly in the case of iridium oxides. A prime example is that of  $\text{Sr}_2\text{IrO}_4$ , for which band theory predicts a metallic ground state, but the combination of spin-orbit coupling and correlations give rise to an antiferromagnetic  $J_{eff} = 1/2$  insulator<sup>1</sup>. This combination of spin-orbit coupling and correlations has proven key to the physics of proposed novel states in the iridates, including superconductivity<sup>2-5</sup>, the Kitaev model<sup>6</sup>, the Weyl semimetal<sup>7-9</sup>, and other topological states<sup>10,11</sup>.

The majority of these exotic states have been typically proposed for iridates in the perovskite  $\text{A}\text{IrO}_3$ <sup>11-14</sup>, layered Ruddlesden-Popper  $\text{A}_{n+1}\text{Ir}_n\text{O}_{3n+1}$ <sup>1,15-17</sup>, and pyrochlore  $\text{A}_2\text{Ir}_2\text{O}_7$ <sup>9,18</sup> structures, where  $A$  is an alkaline earth metal. These different crystal structures share as a common building block  $\text{IrO}_6$  octahedra where the  $\text{Ir}^{4+}$  is in a  $5d^5$  configuration. For example,  $\text{SrIrO}_3$  is a material in which the octahedra form a three dimensional corner sharing network and is proposed to be a topological crystalline insulator with line nodes protected by crystal symmetry<sup>10,11</sup>.  $\text{Sr}_2\text{IrO}_4$  is composed of a two dimensional octahedral network and is proposed to be a novel  $J_{eff} = 1/2$  superconductor upon electron doping<sup>2-5</sup>. Another material which shares the same  $\text{IrO}_6$  ( $5d^5$ ) building block is the rutile polymorph of  $\text{IrO}_2$ . In the perovskite, Ruddlesden-Popper, and pyrochlore structures, the  $\text{IrO}_6$  octahedra are connected in exclusively corner-sharing networks, whereas in the rutile structure, the octahedra exhibit a higher degree of connectivity and are instead tiled with a mixture of both corner and edge sharing neighbors (Fig. 1(a)).  $\text{IrO}_2$  exhibits a number of properties that make it fundamentally interesting and technologically relevant, particularly for spintronic ap-

plications. These include novel magnetotransport, with a large spin Hall angle which clearly highlights the importance of spin-orbit coupling<sup>19</sup>, as well as a Hall effect whose carrier sign can be switched by changing the orientation of the external magnetic field<sup>20</sup>. In addition,  $\text{IrO}_2$  is a very promising catalyst for the oxygen evolution reaction<sup>21,22</sup>. Given its similar *local* structure, one might expect  $\text{IrO}_2$  to share many of the same properties as the other iridates. On the other hand, it is known that subtle structure distortions, such as octahedral tilts, can dramatically alter the properties of complex oxides in general<sup>23</sup>, and perovskite iridates in particular<sup>14</sup>. Therefore, the precise role of electron correlations in determining the properties across iridates with different connectivity remains an open question.

In this Letter, we investigate how the strength of the effective correlations across the iridates varies with the connectivity of the  $\text{IrO}_6$  octahedra using a combination of reactive oxide molecular-beam epitaxy (MBE) synthesis, *in situ* angle-resolved photoemission spectroscopy (ARPES), core level spectroscopy, and density functional theory. In surprising contrast to  $\text{Sr}_2\text{IrO}_4$  and  $\text{SrIrO}_3$ , we find that electron-electron correlations are unusually weak in  $\text{IrO}_2$ , surprising for a transition metal oxide. We discover that the combination of increasing the octahedral connectivity, the metal-oxygen covalency, and the metal-metal interactions reduce the effective correlation strength when going from the antiferromagnetic Mott insulator  $\text{Sr}_2\text{IrO}_4$  to Fermi liquid  $\text{IrO}_2$ , which does not exhibit any appreciable mass enhancement. Thin films of (001)  $\text{SrIrO}_3$ ,  $\text{Sr}_2\text{IrO}_4$ , and (110)  $\text{IrO}_2$  were grown by MBE on  $(\text{LaAlO}_3)_{0.29}(\text{SrAl}_{0.5}\text{Ta}_{0.5}\text{O}_3)_{0.71}$  (LSAT) (001) substrates ( $\text{SrIrO}_3$ ,  $\text{Sr}_2\text{IrO}_4$ ) and  $\text{TiO}_2$  (110) substrates ( $\text{IrO}_2$ ). The films were grown under a background partial pressure of  $10^{-6}$  torr of distilled ozone at a substrate temperature of  $900^\circ\text{C}$  for  $\text{Sr}_2\text{IrO}_4$ ,  $650^\circ\text{C}$  for  $\text{SrIrO}_3$ , and  $350^\circ\text{C}$  for  $\text{IrO}_2$ . Additional details about the growth and characterization of  $\text{SrIrO}_3$  and  $\text{Sr}_2\text{IrO}_4$  can be found in

Ref.<sup>14</sup>. X-ray diffraction (XRD, Cu  $K\alpha$ )  $\theta - 2\theta$  scans confirmed that the  $\text{IrO}_2$  was epitaxial with an out-of-plane  $d_{110}$  spacing of  $3.20(4)$  Å (near the bulk value of  $3.181$  Å<sup>24</sup>, Fig. 1(b)), and have sharp rocking curves (Supplemental). The presence of sharp Kiessig fringes in the XRD pattern indicates that the film was smooth with a thickness of  $16$  nm, in agreement with RHEED oscillations. Following growth, samples were transferred through an ultrahigh vacuum manifold ( $< 3 \times 10^{-10}$  torr) for ARPES measurements which were performed using a VG Scienta R4000 analyzer. For  $\text{IrO}_2$  and  $\text{Sr}_2\text{IrO}_4$ , density functional theory calculations were performed using the generalized gradient approximation including fully relativistic SOC (GGA+SO) in Wien2k<sup>25</sup>. Our calculations are in agreement with a previous DFT+DMFT study<sup>26</sup>. For  $\text{SrIrO}_3$ , calculations were performed within the local density approximation including spin orbit interaction (LDA+SO) using OPENMX as described in Ref.<sup>14</sup>.

We begin with rutile  $\text{IrO}_2$ , where each O is coordinated to three Ir nearest neighbors. In Fig. 1(d), we show the valence band of  $\text{IrO}_2$  using He II photons ( $h\nu = 40.8$  eV) compared to the calculated density of states. The peaks between  $E_F$  and  $3$  eV binding energy are of primarily Ir  $t_{2g}$  character, while the broad bands between  $3$  and  $10$  eV are predominantly O  $2p$  orbitals. The occupied  $t_{2g}$  bandwidth of  $3$  eV for  $\text{IrO}_2$  is significantly broader than that of  $\text{SrIrO}_3$  and  $\text{Sr}_2\text{IrO}_4$  (approximately  $0.3$  and  $0.8$  eV, respectively<sup>14</sup>). Each of the major features in the measured spectrum is remarkably well reproduced by the DFT calculation, and consistent with a previous hard x-ray photoemission study<sup>27</sup>, but with a higher sensitivity to the O  $2p$  states due to the higher relative cross section at low photon energies.

The low-energy electronic structure of  $\text{IrO}_2$  is shown in Fig. 2, measured using He I $\alpha$  photons ( $h\nu = 21.2$  eV), where the energy dispersion curves (EDCs) show sharp quasiparticle (QP) peaks. The dispersion is highly anisotropic and dominated by hole pockets centered at  $(2,0)$   $[(0,0)]$  and  $(1,1)$ , consistent with previous magnetotransport measurements<sup>20</sup>. Given that the peaks in the EDCs are well fit by a Lorentzian lineshape, the width of the momentum distribution curves (MDCs) exhibit an  $\omega^2$  dependence, and the resistivity exhibits a  $T^2$  dependence at low temperatures<sup>28</sup>, these findings indicate that  $\text{IrO}_2$  is well described by a Fermi liquid ground state. To better quantify the strength of the electron-electron correlations, we compare our experimentally extracted dispersions with GGA+SO calculations (excluding any onsite Coulomb repulsion  $U$ ). We find remarkable agreement between our extracted dispersions and GGA+SO, in terms of the Fermi velocity ( $v_F$ ), the Fermi wavevector ( $k_F$ ), and the full occupied bandwidth (Fig. 2(b)). Comparing  $v_F$  for the hole pockets at  $k = (2,0)$  and  $(1,1)$  yields no observable renormalization  $v_{F,DFT}/v_F = 1.0 \pm 0.1$ . Furthermore, the measured occupied bandwidth throughout the Brillouin zone is within ten percent of the DFT values at bind-

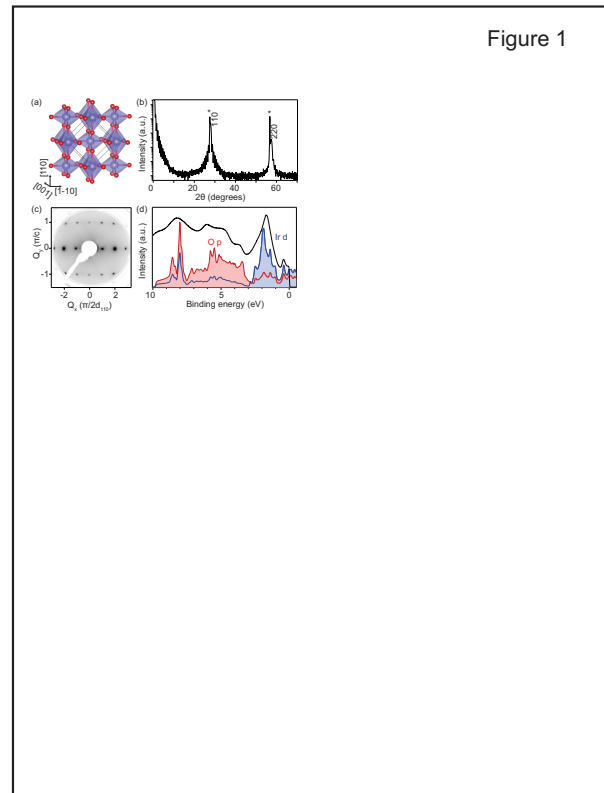


FIG. 1. Crystal structure and valence bands of  $\text{IrO}_2$  (110) films. (a) Crystal structure of rutile, showing chains of edge sharing  $\text{IrO}_6$  octahedra oriented along the  $c$   $[001]$  axis. Ir atoms are in blue, O atoms in red. (b) XRD  $2\theta$  scan of epitaxial  $\text{IrO}_2$  on a  $\text{TiO}_2$  (110) substrate. Substrate peaks are marked by asterisks. (c) Low energy electron diffraction pattern of the  $\text{IrO}_2$  (110) surface measured at  $100$  eV. (d) Momentum-integrated valence band spectrum (black curve,  $k = (1, 0) - (1, 1)$ ) and comparison to GGA+SO partial density of states (shaded).

ing energies extending to larger than  $1$  eV. This level of quantitative agreement between experiment and DFT is remarkable in transition metal oxides, where typically  $m^*/m_{DFT} \approx 2 - 6$ , in material families such as cuprates, nickelates, manganites, titanates, ruthenates, and other iridates<sup>29-34</sup>. From EDC fits of the QP peak, we extract an effective quasiparticle residue of  $Z' = 0.9 \pm 0.1$  (Supplemental), in good agreement with the lack of appreciable velocity renormalization. For comparison, in  $\text{Sr}_3\text{Ir}_2\text{O}_7$ ,  $Z' = 0.25 - 0.5$ <sup>17</sup>. These findings are also consistent with the relatively small Sommerfeld coefficient of  $\gamma = 0.67$  mJ/(mol $\cdot$ K<sup>2</sup>) for  $\text{IrO}_2$  bulk crystals<sup>35</sup>, which is comparable in magnitude to that of simple elemental transition metals.

Comparisons between measurements taken with He I $\alpha$  ( $21.2$  eV) and He II $\alpha$  ( $40.8$  eV) were performed to accurately determine the out-of-plane momentum to be  $k_z =$

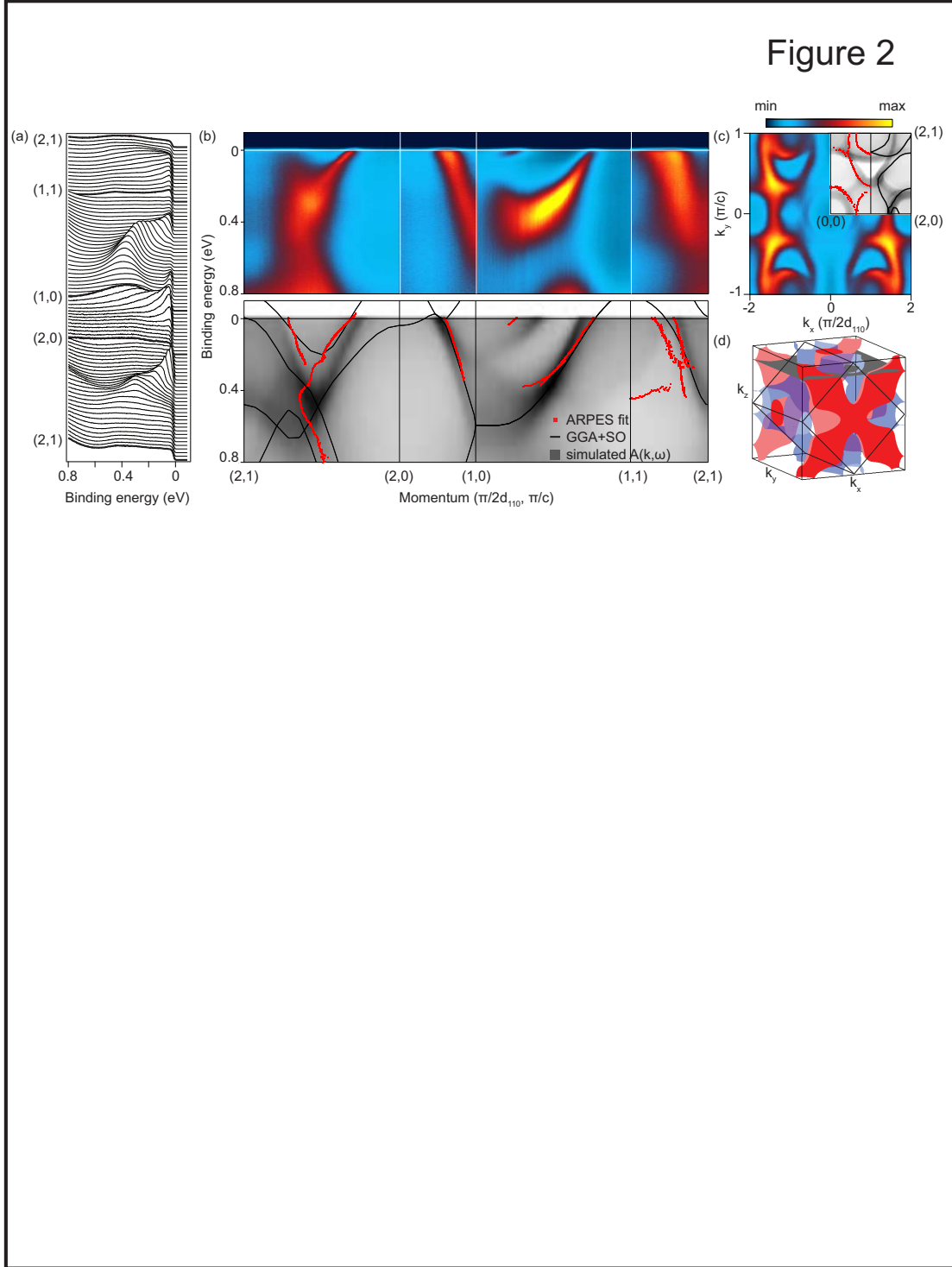


FIG. 2. (a) Energy dispersion curves (EDCs) showing sharp quasiparticle peaks. We define our axes such that  $k_x \parallel [1\bar{1}0]$  and  $k_y \parallel [001]$ , and hence the high symmetry points are expressed in units of  $(\pi/2d_{110}, \pi/c)$ . (b) False-color ARPES intensity (top) and comparison of the extracted dispersions with theory (bottom), for GGA+SO at fixed  $k_z$  and for a simulated spectral intensity with  $k_z$  smearing and lifetime broadening (grayscale). (c) ARPES Fermi surface (color scale), corresponding approximately to a slice through the three dimensional Fermi surface at constant  $k_z$ . The upper right quadrant shows the extracted Fermi surface (red dots) along with the GGA+SO Fermi surface (black lines) and a  $k_z$  broadened simulation (grayscale). (d) Three dimensional Fermi surface.

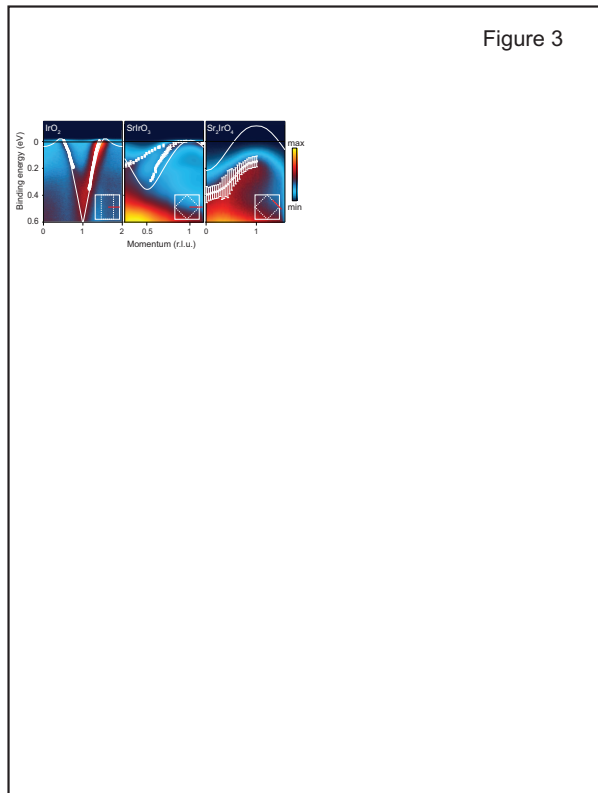


FIG. 3. ARPES intensity (color scale), extracted dispersions (white circles), and DFT+SO (white lines) showing increasing renormalizations from IrO<sub>2</sub> to SrIrO<sub>3</sub> and Sr<sub>2</sub>IrO<sub>4</sub>. Momenta are expressed in units of  $\pi/2d_{110}$ ,  $\pi/a$ , and  $\sqrt{2}\pi/a$ , respectively. The SrIrO<sub>3</sub> and Sr<sub>2</sub>IrO<sub>4</sub> data are adapted from<sup>14</sup>.

$(0.76 \pm 0.05)\pi/d_{110}$ , corresponding to an inner potential of  $U_0 = 11.5$  eV (Supplemental), a value typical for oxides ( $U_0 = 9$  to  $15$  eV<sup>14,36–38</sup>). In Fig. 2(b,lower), we show a simulation of the ARPES spectra at  $k_z = 0.76\pi/d_{110}$  with a smearing of  $\Delta k_z = 1/\lambda$  ( $\lambda \approx 4$  Å is the finite escape depth) and an imaginary self energy broadening of  $Im(\Sigma) = 0.05 + 0.3\omega^2$  eV. The simulation bears a remarkable resemblance to the raw ARPES data in Fig. 2(b,upper), once again suggesting weak electron correlations in IrO<sub>2</sub>. Along  $(1,0) - (1,1)$ , some discrepancies can be observed which we attribute to rapidly dispersing features in  $k_z$  (Supplemental, Fig. S3) which are not fully captured by the  $k_z$  smearing. We also observe two features that are not readily apparent in the GGA+SO calculations, namely a second hole pocket and deep electron pocket with band minimum near 0.4 eV along  $(1,1) - (2,1)$ , which may arise from surface-derived features.

We now compare the effective correlation strength in IrO<sub>2</sub> to other iridates with decreasing connectivity: the perovskite SrIrO<sub>3</sub> (2 Ir atoms coordinated to each O) and layered Sr<sub>2</sub>IrO<sub>4</sub> (1.5 Ir atoms coordinated to each

O). ARPES measurements and extracted dispersions for all three materials are shown in Fig. 3, along with comparison to DFT+SO calculations. As described earlier, in IrO<sub>2</sub> the bandwidth and Fermi velocity do not exhibit observable signs of renormalization compared to the calculation ( $v_{F,DFT}/v_{F,ARPES} = 1 \pm 0.1$ ), while in SrIrO<sub>3</sub> the effective mass of the  $(1,0)$  inner hole pocket is renormalized by a factor of  $m^*/m_{DFT} = 2.0 \pm 0.2$ , and in Sr<sub>2</sub>IrO<sub>4</sub>, DFT+SO does not predict the Mott insulating ground state. Comparing the band curvatures, we find that the bandwidth for Sr<sub>2</sub>IrO<sub>4</sub> is renormalized by a factor  $W/W_{DFT} = 1.35$ . This suggests a clear evolution in the effective correlation strength across the iridates as a function of the connectivity of the IrO<sub>6</sub> octahedra, whose trend is plotted in Fig. 4(c) (black circles). In all cases, the films were thicker than 40 monolayers, much larger than the Thomas-Fermi screening length, and did not have a polar discontinuity at the film/substrate interface. Hence quantum confinement or interfacial effects are expected to be negligible, and thus the ARPES measurements are expected to be comparable to results from a cleaved single crystal.

In addition to the low energy electronic structure measured by ARPES, we also observe systematic changes across the iridates in the Ir  $4f_{5/2}$  and  $4f_{7/2}$  core levels measured *in situ* using Al K $\alpha$  ( $h\nu = 1486.3$  eV, Fig. 4(a)). In all of the iridates, a multi-component peak structure is observed, which arises from a sharp screened  $4f$  doublet (red) and a broader unscreened doublet (blue), which appears at higher binding energy. The relative ratio between the unscreened and screened core levels has been employed as a proxy for measuring the effective strength of correlations across the ruthenates<sup>39</sup>. In our fits, we use a conventional Shirley background (dotted), two Voigt components for each  $4f$  doublet, and a Doniac Sunjic asymmetry parameter to account for the interaction between the core hole and the Fermi sea in metallic IrO<sub>2</sub>. We constrain the ratio of the  $4f_{5/2}$  to  $4f_{7/2}$  weights within each doublet and constrain the spin-orbit splitting to known values. Hence the only free parameters are the relative intensities of the components, their lifetimes, and their binding energy shifts (Supplemental, Table I). In IrO<sub>2</sub>, we find that the  $4f$  core levels are dominated by the sharp screened peak with a relatively small contribution from the unscreened component, also consistent with x-ray photoemission measurements of IrO<sub>2</sub> and RuO<sub>2</sub><sup>27,40</sup>. Moving to SrIrO<sub>3</sub> and Sr<sub>2</sub>IrO<sub>4</sub>, the weight of the screened component decreases while the relative weight of the unscreened component increases; in Sr<sub>2</sub>IrO<sub>4</sub> the spectra are dominated by the unscreened component. This trend is summarized versus octahedral connectivity in Fig. 4(c).

Having established how correlations evolve across the iridates, we now investigate its possible origins. In the DFT+SO densities of states (Fig. 4(b)), the width of the occupied Ir  $t_{2g}$  bands increases when moving from two-dimensional Sr<sub>2</sub>IrO<sub>4</sub> ( $W \approx 1$  eV), to three-dimensional corner sharing SrIrO<sub>3</sub>, to three-dimensional edge and cor-

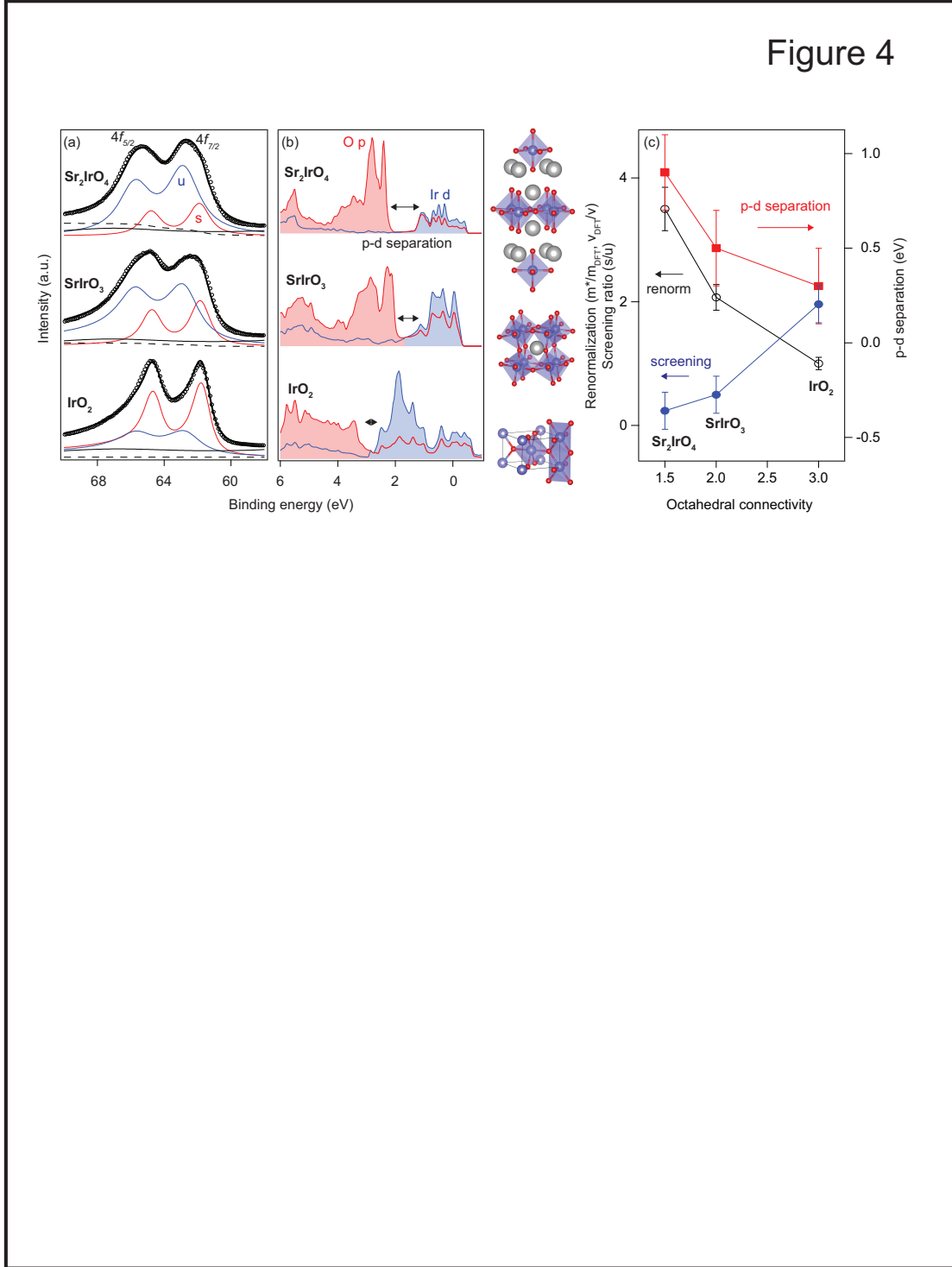


FIG. 4. The connection between structure and correlations across the iridates. (a) Comparison of the Ir  $4f$  and  $5p$  core levels (measurement, open circles), showing screened (s, red) and unscreened (u, blue)  $4f$  components, along with a broad  $5p_{1/2}$  (black). (b) Comparison of the DFT+SO PDOS. The corresponding crystal structures for  $\text{Sr}_2\text{IrO}_4$ ,  $\text{SrIrO}_3$ , and  $\text{IrO}_2$  are shown at the right. (c) Renormalization, Ir  $4f$  screening ratio, and  $p-d$  hybridization versus octahedral connectivity (average number of Ir nearest neighbors coordinated to each oxygen). For the  $\text{IrO}_2$  and  $\text{SrIrO}_3$  renormalizations we use the velocity ( $v_{F,DFT}/v_F$ ) and mass ( $m^*/m_{DFT}$ ) renormalizations, respectively, from our ARPES and DFT+SO. For  $\text{Sr}_2\text{IrO}_4$ , due to the lower statistics of the ARPES measurement we use the mass renormalization from DMFT<sup>31</sup>.

ner sharing  $\text{IrO}_2$  ( $W \approx 3$  eV), which one can consider as a hyper-connected variant of the perovskite structure composed of the same  $\text{IrO}_6$  octahedral building block. Thus, with increasing  $W$ , the ratio  $U/W$  decreases making the effective correlations in  $\text{IrO}_2$  smaller. Furthermore, in  $\text{Sr}_2\text{IrO}_4$ , the density of states exhibits a clear gap ( $\approx 0.9$  eV) separating the Ir  $5d$  and O  $2p$  orbitals (Fig. 4(b)), indicative of a more ionic character, where the conventional picture of oxygen mediated hoppings between the transition metal sites is valid. In this case, the correlations, in conjunction with the spin-orbit coupling, are strong enough to turn the system into a Mott insulator (Fig. 3). In  $\text{SrIrO}_3$ , the density of states shows a small overlap between the  $p$  and  $d$  states and a reduced separation of  $\approx 0.5$  eV (defined as the separation using a tangent line extrapolation to zero of the leading edges of the  $p$  and  $d$  states, see Supplemental), consistent with semimetallic  $\text{SrIrO}_3$  having weaker effective correlations than Mott insulating  $\text{Sr}_2\text{IrO}_4$ . Finally, in metallic  $\text{IrO}_2$ , the density of states shows a further reduction of the  $p-d$  separation ( $\approx 0.3$  eV) and increased overlap between  $p$  and  $d$  states. This leads to a more covalent character, which is also evidenced in tight binding models, for which metal-oxygen covalency parameters are crucial to reproducing the electronic structure of  $\text{RuO}_2$  and  $\text{IrO}_2$ <sup>41</sup>. This covalent hybridization leads to a reduced effective correlation strength, as the spectral weight is shifted onto the more weakly correlated oxygen  $2p$  orbitals as opposed to the more strongly correlated transition metal  $d$  orbitals, thereby resulting in a weaker effective renormalization for  $\text{IrO}_2$ . These trends are also consistent with the Zaanen-Sawatzky-Allen picture<sup>42</sup>, in which the size of the Mott or charge transfer gap is determined by a balance between the on-site Coulomb repulsion  $U$ , the  $p-d$  separation  $\Delta_{p-d}$ , and the  $p-d$  hybridization interaction  $T$ . Although the bare atomic component of the on-site Coulomb repulsion  $U$  should remain largely constant across the iridates, the screened component of  $U$  is decreased by the increased  $p-d$  covalency in  $\text{IrO}_2$ . We argue that this  $p-d$  covalency, as described by  $\Delta_{p-d}$  and  $T$ , is in turn strongly determined by the octahedral connectivity. Finally for  $\text{IrO}_2$ , there is also significant direct bonding between the Ir sites, which is largely insignificant for  $\text{Sr}_2\text{IrO}_4$  and  $\text{SrIrO}_3$ , which provides an additional hopping channel in  $\text{IrO}_2$ , as also suggested from a molecular orbital picture proposed for the rutile struc-

ture at  $d^5$  filling<sup>43</sup>.

A summary of how the low-energy mass (velocity) renormalization ( $m^*/m_{DFT}$ ,  $v_{F,DFT}/v_F$  open black circles), the  $4f$  core hole screening (ratio of screened to unscreened doublets, closed blue circles), and the  $p-d$  separation (red squares) vary as a function of the  $\text{IrO}_6$  octahedral connectivity (the average number of Ir nearest neighbors connected to each oxygen), is shown in Figure 4(c). We find that each of these parameters depends strongly on the structure as parameterized by the octahedral connectivity: the connectivity determines the degree of ionic versus covalent bonding, which in turn determines the correlation induced renormalization and degree of metallicity. Hence the low energy electronic structure of the iridates is not simply set by the local parameters of spin-orbit coupling, band filling, and crystal field splitting alone, but is highly dependent on the octahedral tiling structure in which a high degree of connectivity leads to deviations from the atomic limit, with stronger covalent character and reduced effective correlations. Conversely, recent experimental and theoretical studies suggest in  $5d$  transition metal oxide and fluoride systems with nearly isolated octahedra and thus much narrower bandwidths, the correlations are enhanced, approaching the more idealized  $J_{eff} = 1/2$  limit<sup>44,45</sup>.

In summary, using a combination of MBE, *in situ* ARPES, core level spectroscopy, density functional calculations, and choosing the  $5d^5$  iridates as a model system, we revealed how electron correlations evolve dramatically as a function of octahedral connectivity, from a correlated  $J_{eff} = 1/2$  Mott insulator in  $\text{Sr}_2\text{IrO}_4$ , to a nearly uncorrelated metal in rutile  $\text{IrO}_2$ , and believe this can be generalized across different transition metal oxide families. The ability to accurately quantify the strength of electron correlations should provide important inputs and design considerations for engineering potential correlated electronic materials in artificial correlated materials and heterostructures.

*Acknowledgments.* We thank T. Birol, C. Fennie, C. H. Kim, and Y. F. Nie for fruitful discussions. This work was supported the National Science Foundation through the MRSEC program (Cornell Center for Materials Research, DMR-1120296), the Air Force Office of Scientific Research (Grants No. FA9550-12-1-0335 and FA2386-12-1-3103), and the Office of Naval Research (Grant No. N00014-12-1-0791).

\* kmshen@cornell.edu

† Current address: Department of Materials Science and Engineering, University of Wisconsin, Madison WI 54706

<sup>1</sup> B. J. Kim, H. Jin, S. J. Moon, J.-Y. Kim, B.-G. Park, C. S. Leem, J. Yu, T. W. Noh, C. Kim, S.-J. Oh, et al., Phys. Rev. Lett. **101**, 076402 (2008), URL <http://link.aps.org/doi/10.1103/PhysRevLett.101.076402>.

<sup>2</sup> F. Wang and T. Senthil, Phys. Rev. Lett. **106**, 136402 (2011), URL [http://link.aps.org/doi/10.1103/](http://link.aps.org/doi/10.1103/PhysRevLett.106.136402)

[PhysRevLett.106.136402](http://link.aps.org/doi/10.1103/PhysRevLett.106.136402).

<sup>3</sup> Y. K. Kim, O. Krupin, J. D. Denlinger, A. Bostwick, E. Rotenberg, Q. Zhao, J. F. Mitchell, J. W. Allen, and B. J. Kim, Science **345**, 187 (2014), URL <http://www.sciencemag.org/content/345/6193/187.abstract>.

<sup>4</sup> Y. K. Kim, N. H. Sung, J. D. Denlinger, and B. J. Kim, Nat. Phys. **12**, 37 (2015), URL <http://dx.doi.org/10.1038/nphys3503>.

<sup>5</sup> Y. J. Yan, M. Q. Ren, H. C. Xu, B. P. Xie, R. Tao, H. Y.

- Choi, N. Lee, Y. J. Choi, T. Zhang, and D. L. Feng, *Phys. Rev. X* **5**, 041018 (2015), URL <http://link.aps.org/doi/10.1103/PhysRevX.5.041018>.
- <sup>6</sup> S. H. Chun, J.-W. Kim, H. Z. Jungho Ki and, C. C. Stoumpos, C. D. Malliakas, J. F. Mitchell, K. Mehlawat, Y. Singh, Y. Choi, T. Gog, et al., *Nat. Phys.* **11**, 462 (2015).
- <sup>7</sup> W. Witczak-Krempa, G. Chen, Y. B. Kim, and L. Balents, *Annual Review of Condensed Matter Physics* **5**, 57 (2014), URL <http://dx.doi.org/10.1146/annurev-conmatphys-020911-125138>.
- <sup>8</sup> L. Savary, E.-G. Moon, and L. Balents, *Phys. Rev. X* **4**, 041027 (2014), URL <http://link.aps.org/doi/10.1103/PhysRevX.4.041027>.
- <sup>9</sup> X. Wan, A. M. Turner, A. Vishwanath, and S. Y. Savrasov, *Phys. Rev. B* **83**, 205101 (2011), URL <http://link.aps.org/doi/10.1103/PhysRevB.83.205101>.
- <sup>10</sup> J.-M. Carter, V. V. Shankar, M. A. Zeb, and H.-Y. Kee, *Phys. Rev. B* **85**, 115105 (2012), URL <http://link.aps.org/doi/10.1103/PhysRevB.85.115105>.
- <sup>11</sup> H.-S. Kim, Y. Chen, and H.-Y. Kee, *Phys. Rev. B* **91**, 235103 (2015), URL <http://link.aps.org/doi/10.1103/PhysRevB.91.235103>.
- <sup>12</sup> Y. Chen, Y.-M. Lu, and H.-Y. Kee, *Nat. Commun.* **6**, 6593 (2015), article, URL <http://dx.doi.org/10.1038/ncomms7593>.
- <sup>13</sup> J.-M. Carter, V. V. Shankar, M. A. Zeb, and H.-Y. Kee, *Phys. Rev. B* **85**, 115105 (2012), URL <http://link.aps.org/doi/10.1103/PhysRevB.85.115105>.
- <sup>14</sup> Y. F. Nie, P. D. C. King, C. H. Kim, M. Uchida, H. I. Wei, B. D. Faeth, J. P. Ruf, J. P. C. Ruff, L. Xie, X. Pan, et al., *Phys. Rev. Lett.* **114**, 016401 (2015), URL <http://link.aps.org/doi/10.1103/PhysRevLett.114.016401>.
- <sup>15</sup> M. Uchida, Y. F. Nie, P. D. C. King, C. H. Kim, C. J. Fennie, D. G. Schlom, and K. M. Shen, *Phys. Rev. B* **90**, 075142 (2014), URL <http://link.aps.org/doi/10.1103/PhysRevB.90.075142>.
- <sup>16</sup> J. Kim, A. H. Said, D. Casa, M. H. Upton, T. Gog, M. Daghofer, G. Jackeli, J. van den Brink, G. Khalullin, and B. J. Kim, *Phys. Rev. Lett.* **109**, 157402 (2012), URL <http://link.aps.org/doi/10.1103/PhysRevLett.109.157402>.
- <sup>17</sup> A. de la Torre, E. C. Hunter, A. Subedi, S. McKeown Walker, A. Tamai, T. K. Kim, M. Hoesch, R. S. Perry, A. Georges, and F. Baumberger, *Phys. Rev. Lett.* **113**, 256402 (2014), URL <http://link.aps.org/doi/10.1103/PhysRevLett.113.256402>.
- <sup>18</sup> B.-J. Yang and N. Nagaosa, *Phys. Rev. Lett.* **112**, 246402 (2014), URL <http://link.aps.org/doi/10.1103/PhysRevLett.112.246402>.
- <sup>19</sup> K. Fujiwara, Y. Fukuma, J. Matsuno, H. Idzuchi, Y. Niimi, Y. Otani, and H. Takagi, *Nat. Commun.* **4** (2013), URL <http://dx.doi.org/10.1038/ncomms3893>.
- <sup>20</sup> M. Uchida, W. Sano, K. S. Takahashi, T. Koretsune, Y. Kozuka, R. Arita, Y. Tokura, and M. Kawasaki, *Phys. Rev. B* **91**, 241119 (2015), URL <http://link.aps.org/doi/10.1103/PhysRevB.91.241119>.
- <sup>21</sup> E. Varkaraki, J. Nicole, E. Plattner, C. Comninellis, and C. Vayenas, *J. Appl. Electrochem.* **25**, 978 (1995), ISSN 0021-891X, URL <http://dx.doi.org/10.1007/BF00241594>.
- <sup>22</sup> B. H. Meekins and P. V. Kamat, *J. Phys. Chem. Lett.* **2**, 2304 (2011), URL <http://dx.doi.org/10.1021/jz200852m>.
- <sup>23</sup> J. M. Rondinelli, S. J. May, and J. W. Freeland, *MRS Bulletin* **37**, 261 (2012), ISSN 1938-1425, URL [http://journals.cambridge.org/article\\_S0883769412000498](http://journals.cambridge.org/article_S0883769412000498).
- <sup>24</sup> S. Butler and J. Gillson, *Materials Research Bulletin* **6**, 81 (1971), ISSN 0025-5408, URL <http://www.sciencedirect.com/science/article/pii/0025540871900924>.
- <sup>25</sup> P. Blaha, K. Schwarz, G. K. H. Madsen, D. Kvasnicka, and J. Luitz, *WIEN2K, An Augmented Plane Wave + Local Orbitals Program for Calculating Crystal Properties* (Karlheinz Schwarz, Techn. Universität Wien, Austria, 2001).
- <sup>26</sup> S. K. Panda, S. Bhowal, A. Delin, O. Eriksson, and I. Dasgupta, *Phys. Rev. B* **89**, 155102 (2014), URL <http://link.aps.org/doi/10.1103/PhysRevB.89.155102>.
- <sup>27</sup> J. M. Kahk, C. G. Poll, F. E. Oropeza, J. M. Ablett, D. Céolin, J.-P. Rueff, S. Agrestini, Y. Utsumi, K. D. Tsuei, Y. F. Liao, et al., *Phys. Rev. Lett.* **112**, 117601 (2014), URL <http://link.aps.org/doi/10.1103/PhysRevLett.112.117601>.
- <sup>28</sup> W. D. Ryden, A. W. Lawson, and C. C. Sartain, *Phys. Rev. B* **1**, 1494 (1970), URL <http://link.aps.org/doi/10.1103/PhysRevB.1.1494>.
- <sup>29</sup> E. A. Nowadnick, J. P. Ruf, H. Park, P. D. C. King, D. G. Schlom, K. M. Shen, and A. J. Millis, *Phys. Rev. B* **92**, 245109 (2015), URL <http://link.aps.org/doi/10.1103/PhysRevB.92.245109>.
- <sup>30</sup> A. Koitzsch, S. V. Borisenko, A. A. Kordyuk, T. K. Kim, M. Knupfer, J. Fink, H. Berger, and R. Follath, *Phys. Rev. B* **69**, 140507 (2004), URL <http://link.aps.org/doi/10.1103/PhysRevB.69.140507>.
- <sup>31</sup> R. Arita, J. Kuneš, A. V. Kozhevnikov, A. G. Eguluz, and M. Imada, *Phys. Rev. Lett.* **108**, 086403 (2012), URL <http://link.aps.org/doi/10.1103/PhysRevLett.108.086403>.
- <sup>32</sup> Y. Taguchi, T. Okuda, M. Ohashi, C. Murayama, N. Môri, Y. Iye, and Y. Tokura, *Phys. Rev. B* **59**, 7917 (1999), URL <http://link.aps.org/doi/10.1103/PhysRevB.59.7917>.
- <sup>33</sup> M. B. Salamon and M. Jaime, *Rev. Mod. Phys.* **73**, 583 (2001), URL <http://link.aps.org/doi/10.1103/RevModPhys.73.583>.
- <sup>34</sup> K. M. Shen, N. Kikugawa, C. Bergemann, L. Balicas, F. Baumberger, W. Meevasana, N. J. C. Ingle, Y. Maeno, Z.-X. Shen, and A. P. Mackenzie, *Phys. Rev. Lett.* **99**, 187001 (2007), URL <http://link.aps.org/doi/10.1103/PhysRevLett.99.187001>.
- <sup>35</sup> R. Burriel, E. F. Westrum, and E. Cordfunke, *The Journal of Chemical Thermodynamics* **19**, 1227 (1987), ISSN 0021-9614, URL <http://www.sciencedirect.com/science/article/pii/0021961487900607>.
- <sup>36</sup> Y. Ishida, R. Eguchi, M. Matsunami, K. Horiba, M. Taguchi, A. Chainani, Y. Senba, H. Ohashi, H. Ohta, and S. Shin, *Phys. Rev. Lett.* **100**, 056401 (2008), URL <http://link.aps.org/doi/10.1103/PhysRevLett.100.056401>.
- <sup>37</sup> J. Krempaský, V. N. Strocov, L. Patthey, P. R. Willmott, R. Herger, M. Falub, P. Blaha, M. Hoesch, V. Petrov, M. C. Richter, et al., *Phys. Rev. B* **77**, 165120 (2008), URL <http://link.aps.org/doi/10.1103/PhysRevB.77.165120>.
- <sup>38</sup> K. Saeki, T. Wakita, Y. Muraoka, M. Hirai, T. Yokoya, R. Eguchi, and S. Shin, *Phys. Rev. B* **80**, 125406 (2009), URL <http://link.aps.org/doi/10.1103/PhysRevB.80.125406>.
- <sup>39</sup> H.-D. Kim, H.-J. Noh, K. H. Kim, and S.-J. Oh, *Phys. Rev.*

- Lett. **93**, 126404 (2004), URL <http://link.aps.org/doi/10.1103/PhysRevLett.93.126404>.
- <sup>40</sup> Y. Kim, Y. Gao, and S. Chambers, *Appl. Surf. Sci.* **120**, 250 (1997), ISSN 0169-4332, URL <http://www.sciencedirect.com/science/article/pii/S016943329700233X>.
- <sup>41</sup> L. F. Mattheiss, *Phys. Rev. B* **13**, 2433 (1976), URL <http://link.aps.org/doi/10.1103/PhysRevB.13.2433>.
- <sup>42</sup> J. Zaanen, G. A. Sawatzky, and J. W. Allen, *Phys. Rev. Lett.* **55**, 418 (1985), URL <http://link.aps.org/doi/10.1103/PhysRevLett.55.418>.
- <sup>43</sup> P. I. Sorantin and K. Schwarz, *Inorganic Chemistry* **31**, 567 (1992), URL <http://dx.doi.org/10.1021/ic00030a009>.
- <sup>44</sup> T. Birol and K. Haule, *Phys. Rev. Lett.* **114**, 096403 (2015), URL <http://link.aps.org/doi/10.1103/PhysRevLett.114.096403>.
- <sup>45</sup> B. F. Phelan, J. Krizan, W. Xie, Q. Gibson, and R. J. Cava, *Phys. Rev. B* **91**, 155117 (2015), URL <http://link.aps.org/doi/10.1103/PhysRevB.91.155117>.